Surface structural-chemical characterization of a single-site d^0 heterogeneous arene hydrogenation catalyst having 100% active sites

Linda A. Williams[a], Neng Guo[b], Alessandro Motta[c,d], Massimiliano Delferro[a,1], Ignazio L. Fragalà[c,d,1], Jeffrey T. Miller[b,1], and Tobin J. Marks[a,1]

[a]Department of Chemistry, Northwestern University, Evanston, IL 60208; [b]Chemical Sciences and Engineering Division, Argonne National Laboratory, Argonne, IL 60439; [c]Dipartimento di Scienze Chimiche, Università di Catania, 95125 Catania, Italy; and [d]Consorzio Interuniversitario Nazionale per la Scienza e Tecnologia dei Materiali (INSTM), Unitá di Ricerca di Catania, 95125 Catania, Italy

Contributed by Tobin J. Marks, November 20, 2012 (sent for review August 28, 2012)

Structural characterization of the catalytically significant sites on solid catalyst surfaces is frequently tenuous because their fraction, among all sites, typically is quite low. Here we report the combined application of solid-state ^{13}C-cross-polarization magic angle spinning nuclear magnetic resonance (^{13}C-CPMAS-NMR) spectroscopy, density functional theory (DFT), and Zr X-ray absorption spectroscopy (XAS) to characterize the adsorption products and surface chemistry of the precatalysts $(\eta^5\text{-}C_5H_5)_2ZrR_2$ (R = H, CH_3) and $[\eta^5\text{-}C_5(CH_3)_5]Zr(CH_3)_3$ adsorbed on Brønsted superacidic sulfated alumina (AlS). The latter complex is exceptionally active for benzene hydrogenation, with ∼100% of the Zr sites catalytically significant as determined by kinetic poisoning experiments. The ^{13}C-CPMAS-NMR, DFT, and XAS data indicate formation of organozirconium cations having a largely electrostatic $[\eta^5\text{-}C_5(CH_3)_5]Zr(CH_3)_2^+\cdots AlS^-$ interaction with greatly elongated $Zr\cdots O_{AlS}$ distances of ∼2.35(2) Å. The catalytic benzene hydrogenation cycle is stepwise understandable by DFT, and proceeds via turnover-limiting H_2 delivery to surface $[\eta^5\text{-}C_5(CH_3)_5]ZrH_2(benzene)^+\cdots AlS^-$ species, observable by solid-state NMR and XAS.

surface catalysis | DFT calculations | organometallic chemistry | solid acids

Organometallic molecule-derived heterogeneous catalysts are of increasing interest owing to their enhanced thermal stability and activity vs. their homogeneous analogs, and their atomically precise tailorable metal-ligand structures vs. other heterogeneous catalysts (1, 2). Furthermore, it is becoming increasingly evident that the inorganic support in many systems is noninnocent and can function as both a ligand and an activator, with the chemically important but poorly understood nature of the catalyst–support interaction strongly modulating catalytic activity and selectivity (3, 4). When adsorbed on Lewis acidic, dehydroxylated alumina surfaces, group 4 complexes such as Cp_2ZrR_2 (Cp = η^5-C_5H_5; **A**, R = H; **B**, R = CH_3) and Cp*Zr$(CH_3)_3$ [**C**, Cp* = η^5-$C_5(CH_3)_5$] were argued on the basis of high-resolution solid-state NMR spectroscopy to transfer an alkyl anion to unsaturated, Lewis acidic surface sites as in Fig. 1 (complexes **B**, **C** → qualitative model **D**) (5, 6). The resulting catalysts are extremely active for olefin hydrogenation and polymerization, and analogous ion-paired species form the basis for large-scale industrial polymerization processes (7, 8). However, kinetic poisoning experiments in which the catalytic sites are titrated in situ with H_2O or ^{t}BuCH$_2$OH indicate that ≤5% of **D**-type sites are catalytically significant, likely reflecting, among other factors, the established heterogeneity of alumina surfaces (5, 6, 9), hence rendering active site structural and chemical descriptions necessarily imprecise. In contrast to these results, chemisorption of such organozirconium precursors on SiO_2, Al_2O_3, and SiO_2-Al_2O_3 surfaces having appreciable coverage by weakly acidic OH groups predominantly yields covalently bound, poorly electrophilic **E**-type species via Zr–CH_3 protonolysis with CH_4 evolution (5, 6, 10, 11). Although the **E**-type sites may be characterized in some detail by high-resolution solid-state NMR and extended X-ray adsorption fine structure spectroscopy (EXAFS), they display minimal catalytic turnover in the absence of added, complicating activators [e.g., methylalumoxane or $B(C_6F_5)_3$], and the fraction of catalytically significant sites is unknown (12, 13). In such situations, it is experimentally impossible to unambiguously distinguish catalytically significant sites from inactive "spectator" sites, hence to fully understand the catalytic chemistry.

In marked contrast to the above results, chemisorption of these same organozirconium molecules on highly Brønsted "superacidic" sulfated metal oxides (14–16) such as sulfated zirconia (ZrS, $H_0 = -16.1$), sulfated titania (TiS, $H_0 = -14.6$), or sulfated alumina (AlS, $H_0 = -14.6$) yields, via Zr–CH_3 protonolysis with methane evolution, highly electrophilic adsorbate species that tentatively have been assigned **F**-type structures (Fig. 1) (17, 18). Here, H_0 is the standard Hammett acidity function, determined spectroscopically, by reactivity, or by temperature-programmed desorption/reaction (14–16). Remarkably, adsorbate structure **C**/**AlS** is one of the most active arene hydrogenation catalysts yet discovered, and by kinetic poisoning experiments, 97 ± 2% and 87 ± 3% of the Zr centers are catalytically significant for benzene hydrogenation and ethylene polymerization, respectively (17, 18). This unusually high percentage of catalytically significant d^0 sites, the relatively clean adsorption/activation chemistry, and the unusual catalytic properties present a unique opportunity to structurally characterize such electrophilic surface catalyst structures in quantitative detail, hence to understand the origin of the unusual catalytic properties. Herein we report a combined ^{13}C-cross-polarization magic angle spinning nuclear magnetic resonance (^{13}C-CPMAS-NMR) spectroscopic, periodic density function theory (DFT) computational, and Zr K-edge XAS structure/reactivity characterization study of these supported organozirconium cations having nearly 100% active sites, and the informative active catalyst structural/catalytic chemistry description that emerges.

Results and Discussion

Complexes **B** and **C** were prepared, purified, and chemisorbed on AlS with rigorous exclusion of oxygen and moisture, using techniques described elsewhere (*Materials and Methods*) (3, 17, 18). Studies of **C**/**AlS**-mediated benzene hydrogenation were carried out as described in *SI Materials and Methods*, under conditions minimizing mass transport effects (3, 17, 18). The turnover frequency (N_t) for benzene hydrogenation at 25.0(±1) °C/1.0 atm H_2 is measured to be 120 (mol benzene)(mol Zr)$^{-1}\cdot$h^{-1}, in good agreement with previously reported data (17, 18). As a

Author contributions: M.D., I.L.F., J.T.M., and T.J.M. designed research; L.A.W., N.G., A.M., and M.D. performed research; M.D., I.L.F., J.T.M., and T.J.M. contributed new reagents/analytic tools; M.D., I.L.F., J.T.M., and T.J.M. analyzed data; and A.M., M.D., and T.J.M. wrote the paper.

The authors declare no conflict of interest.

[1]To whom correspondence may be addressed. E-mail: t-marks@northwestern.edu, m-delferro@northwestern.edu, lfragala@dipchi.unict.it, or millerjt@anl.gov.

This article contains supporting information online at www.pnas.org/lookup/suppl/doi:10.1073/pnas.1220240110/-/DCSupplemental.

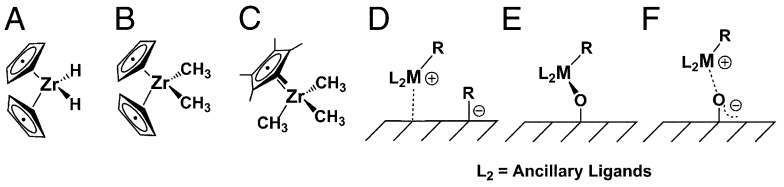

Fig. 1. Proposed model structures of chemisorbed organozirconium complexes A (*A*), B (*B*), and C (*C*) on (*D*) dehydroxylated Lewis acidic metal oxides, (*E*) weakly Brønsted acidic hydroxylated metal oxides, and (*F*) highly Brønsted acidic sulfated metal oxides.

control, studies of benzene hydrogenation in homogenous solution using $Cp^*Zr(CH_3)_3 + B(C_6F_5)_3$ or $Cp^*Zr(CH_3)_3 + Ph_3C^+B(C_6F_5)_4^-$ catalysts yield N_t = 1–2 (mol benzene)(mol Zr)$^{-1}\cdot h^{-1}$, highlighting the dramatic role that chemisorption on this particular support plays in the catalysis. Furthermore, negligible turnover occurs on the sulfated oxides in the absence of chemisorbed complex **C**. To our knowledge, the only other supported early-transition metal catalysts active for arene hydrogenation are M[μ-CSi$(CH_3)_3$][$CH_2Si(CH_3)_3$]$_2$/SiO_2 (M = Nb, Ta), where N_t = 800 (mol benzene)(mol Nb)$^{-1}\cdot h^{-1}$ and 333 (mol benzene)(mol Ta)$^{-1}\cdot h^{-1}$) under far more drastic conditions (120 °C, 80–95 atm H_2), and little is known about their structures (19).

Chemisorption of ^{13}C-labeled $Cp^*Zr(^{13}CH_3)_3$ (**C′**) and $Cp^*Zr(CH_3)_3$ (**C**) onto AlS, dosing of **C/AlS** with 10% (vol/vol) ^{13}C-enriched benzene (*SI Materials and Methods*), and the structure of **C/AlS** after benzene hydrogenation were first investigated by solid-state ^{13}C-CPMAS-NMR spectroscopy. The spectra of **C′/AlS** and **C/AlS** (Fig. 2 *A* and *B*, respectively), exhibit three major resonances at δ 122.8, 49.7, and 9.2 ppm, with those at δ 122.8 and 9.2 straightforwardly assigned to Cp* framework and Cp*-*C*H_3 carbon atoms (6, 17, 18), whereas the downfield shifted Zr–CH_3 signal at δ 48.9 ppm indicates formation of a "cation-like" electron-deficient organozirconium species (20, 21), and negligible amounts of alkyl anion transfer to a quadrupolar Al site (Al-$^{13}CH_3^-$; as in structure **D**) (17, 18, 21). After exposing a pentane slurry of **C′/AlS** to H_2 (*SI Materials and Methods, Hydrogenolysis of* ***Cp*Zr^{13}Me$_3$/AlS*** and Fig. S1), the downfield Zr–$^{13}CH_3$ signal at δ 48.9 ppm disappears, whereas the resonances associated with the Cp* ligand are unchanged, indicating formation of a catalytically active cationic Cp*Zr–hydride species (20–23). The ^{13}C chemical shift of ^{13}C-enriched benzene physisorbed on AlS is assigned at δ 120.3 ppm (Fig. 2*C*) (24), whereas exposure of **C/AlS** to ^{13}C-enriched benzene yields a downfield shifted resonance at δ 127.5 ppm, consistent with benzene coordination to a cation-like d^0 species (Fig. 2*D*) (25–27). Subsequent treatment of this species with substoichiometric H_2 in a benzene slurry yields a signal assignable to cyclohexane at δ 28.5 ppm, presumably physisorbed on the AlS surface (Fig. 2*E* and *SI Materials and Methods, Benzene Hydrogenation Experiment with* ***Cp*ZrMe$_3$/AlS***). The breadth of the Cp* resonance suggests that some benzene molecules are still coordinated to the Zr center [see the discussion on EXAFS below].

Molecular catalyst–surface interactions were modeled next using the DFT periodic formalism (28) (*SI Materials and Methods*), beginning with the AlS surface. First, it is found that the AlS surfaces expose two predominant sulfate species, sites $\mathbf{S_A}$ and $\mathbf{S_B}$ (Fig. S2), as well as $(Al)_nOH$ hydroxyl groups, in which the OH is coordinated either to three Al (n = 3, O3 in Fig. S2) or to two Al ions (n = 2, O2 in Fig. S2). The formation of $\mathbf{S_A}$ sites involves a double-exchange/condensation reaction with the surface and does not afford an acidic proton, whereas $\mathbf{S_B}$ arises from a single exchange/condensation reaction with the surface, preserving one acidic proton that is then transferred to an Al-O surface site via an acid/base exchange process. Surface Brønsted acid properties and computed ν(S = O) vibrational modes, both before and after organozirconium complex chemisorption, are in good agreement with the experiment (17, 18). In principal, the precursor Zr–CH_3 protonolysis/chemisorption may occur at either a surface $(Al)_2O(2)H$ or an $(Al)_3O(3)H$ site. The DFT results indicate that Zr–CH_3 protonolysis is favored at the $(Al)_3O(3)H$ site owing to the greater Brønsted acidity, which may be quantified by the relative computed stabilities of the anionic surfaces

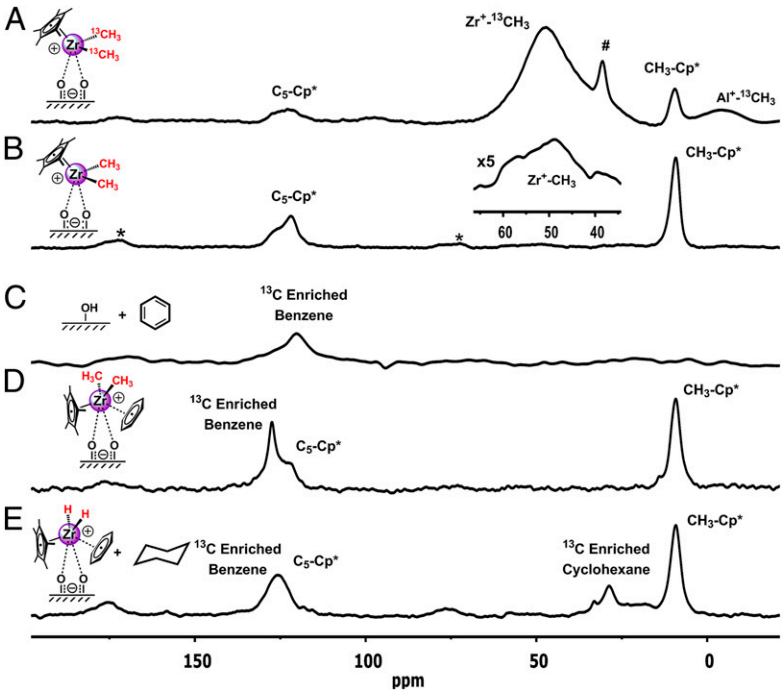

Fig. 2. Solid-state ^{13}C-NMR spectra of organozirconium species on sulfated aluminum oxide. ^{13}C-CPMAS-NMR spectra (100-MHz, 16K scans; repetition time, 5 s; contact time, 2 ms; spinning speed, 5 kHz) of (*A*) $Cp^*Zr(^{13}CH_3)_3$, **C′/AlS**; (*B*) $Cp^*Zr(CH_3)_3$, **C/AlS**; (*C*) ^{13}C-enriched benzene physisorbed on AlS; (*D*) **C/AlS/H$_2$** exposed to ^{13}C-enriched benzene; and (*E*) **C/AlS** after ^{13}C-enriched benzene hydrogenation. *Rotational sidebands; #, impurity.

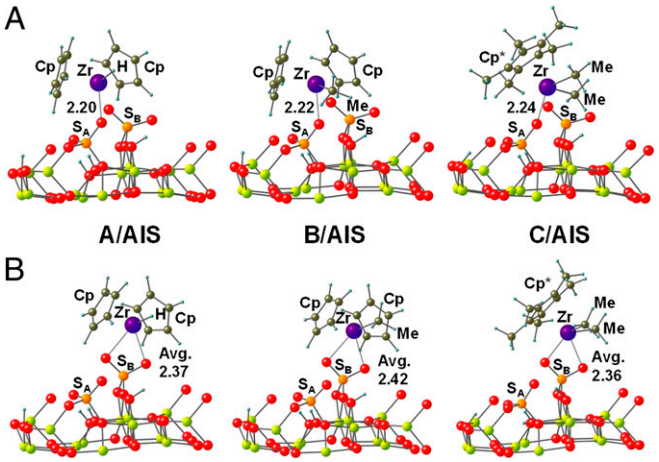

Fig. 3. Energy-minimized computed chemisorbed catalyst structures for (*A*) Cp_2ZrH^+ (complex **A**), Cp_2ZrMe^+ (complex **B**), and $Cp^*Zr(CH_3)_2^+$ (complex **C**) coordination to the S = O groups of the sulfated alumina surface at $\mathbf{S_A}$ sites, and (*B*) Cp_2ZrH^+ (**A**), Cp_2ZrMe^+ (**B**), and $Cp^*Zr(CH_3)_2^+$ (**C**) coordination to the S = O groups of the sulfated alumina surface at $\mathbf{S_B}$ sites. Distances in angströms (Å). Al, yellow-green; Avg, average distance; C, olive; H, blue; O, red; S, orange; Zr, purple.

formed on deprotonation. The chemisorbed organozirconium surface species were next modeled for complexes **A**–**C** by placing the cationic species on the anionic/deprotonated AlS surface and seeking energy-minimized structures, as shown in Fig. 3. In all cases, two structures with similar energetic stabilizations are located, arising from the interaction between the Zr cation and sulfate species $\mathbf{S_A}$ and $\mathbf{S_B}$. Any attempt to simulate the interaction of a Zr cation with a surface $(Al)_nO^-$ species fails because of the sterically encumbered approach of the Zr metal-ligand complex to the surface. For all adsorbate complexes investigated, the interaction with $\mathbf{S_A}$ forms structures with rather long computed Zr···O distances of 2.20 Å, 2.22 Å, and 2.24 Å for complexes **A**, **B**, and **C**, respectively. Alternatively, when the interaction involves surface $\mathbf{S_B}$ units, the cationic Zr complex lies between two S = O groups with computed Zr···O mean distances of 2.37 Å, 2.42 Å, and 2.36 Å for complexes **A**, **B**, and **C**, respectively (Fig. 3). The different computed Zr···O distances are ascribable to the differing electronic and steric characteristics of the **A**–**C** ligands. As is discussed below, these results are in good agreement with the EXAFS data, and represent significantly longer distances than in typical molecular covalent Zr(IV)-OR bonds (1.94–2.01 Å),† suggesting very weak ion pairing. Moreover, the computational models of **C/AlS** yield $Cp^*Zr(CH_3)_2^+\cdots O_{AlS}^-$ structures in excellent agreement with the present solid-state NMR spectroscopic data and NMR data for metallocenium electrophiles in solution (20, 26, 29).

Finally, for all chemisorbed complexes, the DFT-derived internal organometallic catalyst metrical parameters were investigated and found to be very similar to those in the respective precatalyst molecules. Only minor distortions of the neutral molecule bond lengths and bond angles are observed, and these accommodate closer cation approach to the surface. Structural parameters for **A/AlS**, **B/AlS**, and **C/AlS** are summarized in Table 1. Similar patterns are observed in comparing the single-crystal diffraction-derived molecule structures of analogous ion pairs vs. their neutrally charged molecular precursors (†, 30).

Zr K-edge EXAFS and X-ray absorption near-edge structure (XANES) data for the neat and supported complexes were collected using strictly anhydrous/anaerobic methodology (31). Attempts to fit the **C/AlS** EXAFS spectrum with models involving four scattering shells, Zr–C(Cp*), Zr–CH_3(Cp*), Zr–CH_3, and Zr–O, were complicated by the overlap of the scatterers arising from the insignificant differences in both bond distances and scattering characteristics (phase and amplitude). Therefore, to better define catalyst structural details, the EXAFS spectra were analyzed by fitting the difference spectra of the organozirconium complexes before and after chemisorption on AlS, after exposure to benzene (Fig. S3), and after benzene hydrogenation (Fig. S4), thus retaining only the new scattering contributions associated with the structural changes while eliminating invariant contributions (*Materials and Methods*) (31, 32). In this way, the Cp_2ZrH_2 spectrum was used to isolate the scattering contributions of the Cp_2Zr fragment. To validate the EXAFS accuracy of the FEFF-generated phase shifts and backscattering amplitudes (33) for Zr–C scattering, compound **A** (Cp_2ZrH_2) with a single Zr–C scattering shell (Cp) first was examined. The spectrum of neat **A** and the fitted spectrum are shown in Fig. 4*A*, and relevant data are compiled in Table 2. The derived coordination number of 10.1 (two η^5-C_5H_5 rings) is within the 10% uncertainty associated with EXAFS techniques (31, 32), whereas the derived average Zr–C distance of 2.52(±2) Å falls within the 2.39–2.58-Å Zr–C(Cp) bond distance range for numerous Cp_2ZrX_2 complexes (20, 34, 35). Compound **B** [$Cp_2Zr(CH_3)_2$] with two distinct Zr–C scattering shells (Cp and CH_3) similarly was characterized, and the spectrum can be fit to a model with 2.1 and 10.3 C atoms at distances from Zr of 2.27 (±2) Å and 2.53(±2) Å, respectively (Table 2). These parameters are in excellent agreement with single-crystal diffraction data for **B**, where Zr–CH_3 = 2.276(5) Å and Zr–C(Cp) = 2.525(±12) Å (20, 35), and lend confidence in the present data analysis procedure. Fitting the difference EXAFS spectrum of **B/AlS** – **B** (Fig. 4*B*) as above reveals that the Zr–O scattering contribution in supported catalyst **B/AlS** involves 2.1 O atoms at an average Zr–O distance of 2.37(±2) Å. There is no evidence of a close Zr···Zr contact as might be expected for a dimeric species. These results are in excellent agreement with the aforementioned DFT models of $\mathbf{B/S_B}$ (Fig. 3*B*), which yield an average Zr···O bond distance of 2.37 Å, significantly longer than in typical molecular covalent Zr–O bonds, as noted above.

XAS-monitored catalytic experiments next were carried out in which **C/AlS** was exposed to benzene, then H_2 at 25 °C. Fig. 4*C* compares the XANES data for $\mathbf{C{\cdot}C_6H_6/AlS}$ with those of **C/AlS**. Note that $\mathbf{C{\cdot}C_6H_6/AlS}$ exhibits a shift in the edge to higher energy of about 0.8 eV (18.0013 keV with chemisorbed benzene vs. 18.0005 keV without benzene) broadening of the XANES beyond the edge vs. untreated **C/AlS**, consistent with benzene coordination. Although Zr K-edge XANES (corresponding to a 1*s* to 5*p* orbital electronic transition) does not probe the *d*-band structure directly, and is thus less sensitive to changes in the coordination environment, it is reasonable that benzene π^*

Table 1. DFT-computed geometrical parameters (angströms and degrees) for catalysts Cp_2ZrH_2, Cp_2ZrMe_2, and Cp^*ZrMe_3 chemisorbed on sulfated alumina

	Cp_2ZrH_2		Cp_2ZrMe_2		Cp^*ZrMe_3	
	$\mathbf{S_A}$	$\mathbf{S_B}$	$\mathbf{S_A}$	$\mathbf{S_B}$	$\mathbf{S_A}$	$\mathbf{S_B}$
Zr–H	1.82	1.82				
Zr–CH_3			2.26	2.29	2.24*	2.24*
Zr–Cp_{center}	2.19*	2.20*	2.22*	2.22*	2.20	2.21
Zr–C(Cp)	2.51	2.51	2.53	2.53	2.51	2.51
Zr–O = S	2.20	2.37*	2.22	2.42*	2.24	2.36*
∠Cp1-Zr-Cp2	133.4	133.1	129.6	131.2		
∠Me1-Zr-Me2					100.3	99.3
∠Cp1-Zr-Cp2-CH_3			60.4	65.6		
∠Cp1-Zr-Cp2-H	73.4	77.4				

*Average values reported. ∠, angle.

†The average distance found in the Cambridge Crystallographic Data Centre (CDC, Feb. 2012) for Zr–O single bonds is 2.000 (±2).

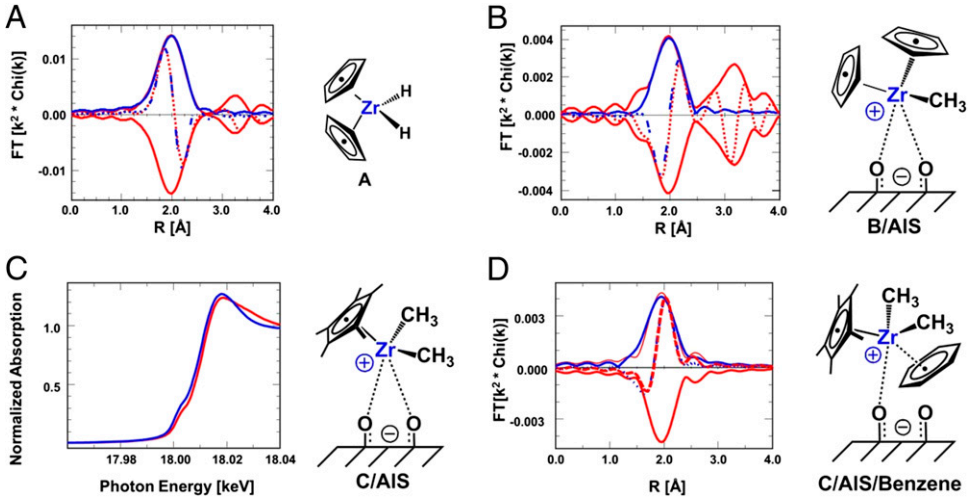

Fig. 4. k^2-weighted Fourier transforms (FT) of organozirconium complex Zr K-edge EXAFS. (*A*) k^2-weighted Fourier transforms of neat Cp_2ZrH_2 (complex **A**). Red, Δk = 2.5–10.0 $Å^{-1}$ data; blue, fit ($N_{Zr\text{-}Cp}$ = 10.1 at 2.52 Å) for ΔR = 1.4–2.6 Å; solid line, FT magnitude; dotted line, FT imaginary part. (*B*) k^2-weighted Fourier transform of the Zr K-edge EXAFS of **B/AlS − B**. Red, Δk = 2.5–10.2 $Å^{-1}$ data; blue, fit ($N_{Zr\text{-}O}$ = 2.1 at 2.37 Å) for ΔR = 1.5–2.6 Å; solid line, FT magnitude; dotted line, FT imaginary part. (*C*) Zr K-edge XANES from 17.96 to 18.04 keV. Red, **C/AlS** + benzene (E_o = 18.0013 keV); blue, **C/AlS** (E_o = 18.0005 keV). (*D*) k^2-weighted Fourier transform of the Zr K-edge difference EXAFS of **C·C$_6$H$_6$/AlS − C/AlS**. Red, Δk = 2.7–10.6 $Å^{-1}$ data; blue, fit for ΔR = 1.6–2.3 Å ($N_{Zr\text{-}Bz}$ = 3.0 at 2.35 Å); solid line, FT magnitude; dotted line, FT imaginary part.

orbital–Zr 5*p* orbital mixing would provide additional transition probability for the Zr 1*s* core electrons, leading to the observed spectral changes (36). More interestingly, as shown in Fig. 4*D* (and summarized in Table 2), fitting of the **C·C$_6$H$_6$/AlS − C/AlS** difference EXAFS spectrum reveals that each Zr center has obtained ~3.0 additional carbon neighbors. In principle, this coordination might correspond to possible scenarios: (*i*) ~50% of the organozirconium centers are coordinated to benzene in an η^6-coordination fashion; (*ii*) ~100% of the active sites are coordinated to benzene in an η^3 mode; or (*iii*) metal coordination induces significant benzene ring deformation from planarity (37). The last hypothesis, however, is not supported by the EXAFS metrical data. Furthermore, the average EXAFS-derived Zr–$C_{benzene}$ distance is 2.35(±2) Å, in good agreement with single-crystal diffraction-characterized benzene coordination to electrophilic d^0 centers (27, 38). Although η^3 coordination is relatively uncommon for π-complexed arenes (39, 40), the present results are consistent with the solid-state NMR results and DFT calculations, considering the overlap of four scattering shells.

The DFT models of the **C·C$_6$H$_6$/AlS** structure indicate that the benzene fragment has inserted between the Zr···O contacts at either site $\mathbf{S_A}$ or site $\mathbf{S_B}$ and engages in η^n benzene coordination (Fig. 5*A*), with three Zr–C(benzene) distances (Zr–C1, Zr–C2, and Zr–C6) slightly shorter than the others by ~0.05 Å. Thus, the computed Zr–C(benzene) mean distance is found to be 2.71 Å, somewhat overestimated vs. the EXAFS-derived distance [2.35 (±2) Å] and the average distance for cationic Zr(IV)–η^6-benzene complexes [2.62(±2) Å] in the Cambridge Crystallographic Database (34). This is not completely unexpected, and in other combined DFT + EXAFS studies, DFT calculations sometimes have overestimated bond distances (41–43). As a consequence of the benzene coordination, the Zr centers of chemisorbed species $\mathbf{C/S_A}$ and $\mathbf{C/S_B}$ are displaced substantially from the anionic surface coordination sites $\mathbf{S_A}$ and $\mathbf{S_B}$, respectively, and the **C•C$_6$H$_6$/AlS** structure converges to a unique conformation in which the cationic complex lies between the $\mathbf{S_A}$ and $\mathbf{S_B}$ vicinal sulfate groups (Fig. 5*A*). A long contact between the Zr center and the $\mathbf{S_B}$ surface site is observed with a Zr···O($\mathbf{S_B}$) distance of 4.17 Å. With the benzene inserted between the cationic Zr center and the $\mathbf{S_A}$ anion, the Zr···O($\mathbf{S_A}$) distance is elongated even further to 5.21 Å. This benzene insertion/activation process is calculated to be exothermic by ~14 kcal/mol with respect to $\mathbf{C/S_B}$, and ~4 kcal/mol with respect to $\mathbf{C/S_A}$. Interestingly, the arene intrusion between the cationic Zr-alkyl center and the weakly coordinating anionic surface is reminiscent of the ethylene coordination/activation mode at homogeneous cationic single-site catalyst centers and fluoroarylborate counteranion displacement that precedes monomer enchainment and polymerization (Fig. 5*B*) (44–46).

Following substoichiometric benzene hydrogenation (*Materials and Methods*), fitting of the (**C·C$_6$H$_6$/AlS** + H_2) − **C·C$_6$H$_6$/AlS** EXAFS difference spectrum reveals that about 50% of the Zr sites retain a coordinated benzene molecule [CN = 1.6; Zr–$C_{benzene}$ = 2.36(±2) Å], in good agreement with the aforementioned ^{13}C-CPMAS NMR results (Fig. 2*E*) and kinetic data showing that benzene is irreversibly captured by **C/AlS**, that the established rate law is zero-order in [benzene], and that the first H_2 addition is turnover limiting (17, 18). The pathway for the present, highly unusual d^0-mediated arene hydrogenation process next was probed by DFT. The calculations (Fig. 6) reveal that the initial **C•C$_6$H$_6$/AlS** hydrogenation/activation, involving Zr–CH_3^+ hydrogenolysis to produce the active catalyst,

Table 2. EXAFS data for neat and supported organozirconium complexes

Entry	Complex	Scatterer	CN (±10%)	R (±0.02 Å)	$\Delta\sigma^2$ ($Å^2 \times 10^3$)	E_0 (eV)
1	**A**	Zr–Cp	10.1	2.52	0.0	0.3
2	**B**	Zr–CH_3	2.1	2.27	−3.0	2.0
		Zr–Cp	10.3	2.53	0.0	0.4
3	**B/AlS − B**	Zr–$O_{support}$	2.1	2.37	−3.0	10.8
4	**C·C$_6$H$_6$/AlS − C/AlS**	Zr–$C_{benzene}$	3.0	2.35	2.0	11.6
5	**C·C$_6$H$_6$/AlS − C·C$_6$H$_6$/AlS/H$_2$**	Zr–$C_{benzene}$	1.6	2.36	2.0	9.7

Cp*ZrH$_2$•C$_6$H$_6$/AlS, is exothermic by ~38 kcal/mol, in agreement with the aforementioned NMR data (Fig. 2). As a consequence of the lesser Zr–H steric hindrance vs. Zr–CH$_3$, the metal center is drawn toward the **S$_B$** surface sites to afford a somewhat closer Zr···O contact of 2.32 Å. The initial step of the catalytic cycle consists of formal H$^-$ transfer from Zr center to the activated arene and formation of a formal Zr–C σ-bond (**I**). A coordination site around the Zr center remains open, and the Zr···O(**S$_B$**) distance contracts to 2.18 Å, whereas the interaction with **S$_A$** is lost. The second step in the catalytic cycle involves H$_2$ activation (**II**) with slight elongation of Zr···O(**S$_B$**) to 2.30 Å, followed by Zr–C hydrogenolysis (**III**) to regenerate a Zr hydride. To achieve complete benzene hydrogenation, appropriate variants of the **I→II→III** sequence are repeated to ultimately produce cyclohexane. The potential energy and Gibbs free-energy profiles for this cycle, depicted in Fig. 6*B*, indicate that thermal and entropic contributions are most important in the benzene and H$_2$ activation steps and in the product release. In the former, this primarily reflects entropy changes associated with the bimolecularity, whereas opposite considerations hold for the product release. Note that the initial benzene capture remains exergonic because of the stronger binding vs. H$_2$, whereas the free-energy gain associated with H$_2$ activation is 2.4, 12.5, and 5.9 kcal/mol for the first, second, and third hydrogenation subcycles, respectively. These differences reflect small displacements of the Zr center from the surface, as required for H$_2$ binding. To locate the turnover-limiting step, we focused on the transition-state energies associated with the most relevant steps of the catalytic cycle (*SI Materials and Methods*). The results reveal that benzene coordination and intramolecular hydride transfer (step **I**) essentially are barrierless processes, whereas H$_2$ activation (step **II**) presents a significant barrier (17.0 kcal/mol) and for the Zr–C hydrogenolysis (step **III**), it is necessary to overcome a 3.5-kcal/mol energy barrier to break the H–H bond. These results point to the H$_2$ activation (step **II**) as the turnover-limiting step of the overall benzene hydrogenation cycle, in accord with the aforementioned experimental observations that the rate law is zero-order in [benzene] and first-order in [H$_2$], and with observations on a related organothorium/alumina system (5). In that case, D$_2$ is delivered in pairs to both arene faces, meaning that arene "flipping over" and/or rapid hydrogenate dissociation/reassociation are possible, but neither cyclohexene nor cyclohexadiene are present in detectable quantities during turnover.

Conclusions

The present results provide a unique combined ^{13}C-CPMAS NMR, DFT computational, and XAS picture of how molecule-derived d^0 organozirconium arene hydrogenation catalysts are activated and turn over on sulfated oxide surfaces. The long Zr$^+$···O$_{AlS}^-$ distances indicate loose, nondirectional ion pairing, as might be expected from the conjugate base of an extremely strong solid Brønsted acid in which the negative charge is highly dispersed (15, 16), and finds surprisingly close analogy to homogeneous ion-paired early-transition metal polymerization catalysts in which the nature of the ion pairing between the cationic catalyst and the charge-dispersed, electrostatically bound, and easily displaceable counteranion strongly modulates the barrier to olefin activation and enchainment (44–47). Indeed, this description is closely analogous to Fig. 5*B*, in which the initial activation of the incoming olefinic substrate by the electrophilic metal center requires geometrical loosening of the ion pairing (46–48). From a coordination chemistry perspective, this also suggests the intriguing possibility that such electron-deficient surfaces may be the long-sought, ultimate "weakly coordinating" anions.

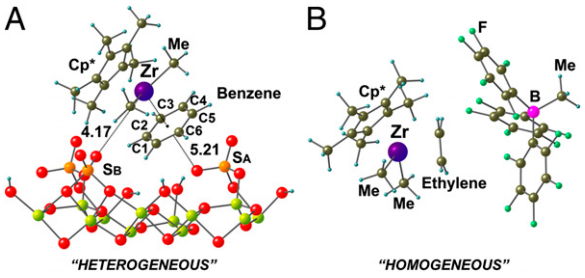

Fig. 5. Energy-minimized computed structures of surface-bound and solution-phase catalyst–substrate complexes. (*A*) Cp*Zr(CH$_3$)$_2^+$ cation coordination to/activation of a benzene molecule and an S = O fragment of an anionic surface sulfate group at two different AlS sites (**C·C$_6$H$_6$/AlS**). (*B*) Cp*Zr(CH$_3$)$_2^+$ cation coordination to/activation of an ethylene molecule, which has displaced an H$_3$CB(C$_6$F$_5$)$_3^-$ counteranion in homogeneous solution. Distance in angströms (Å). Al, yellow; B, pink; C, olive; F, green; H, blue; O, red; S, orange, Zr, purple.

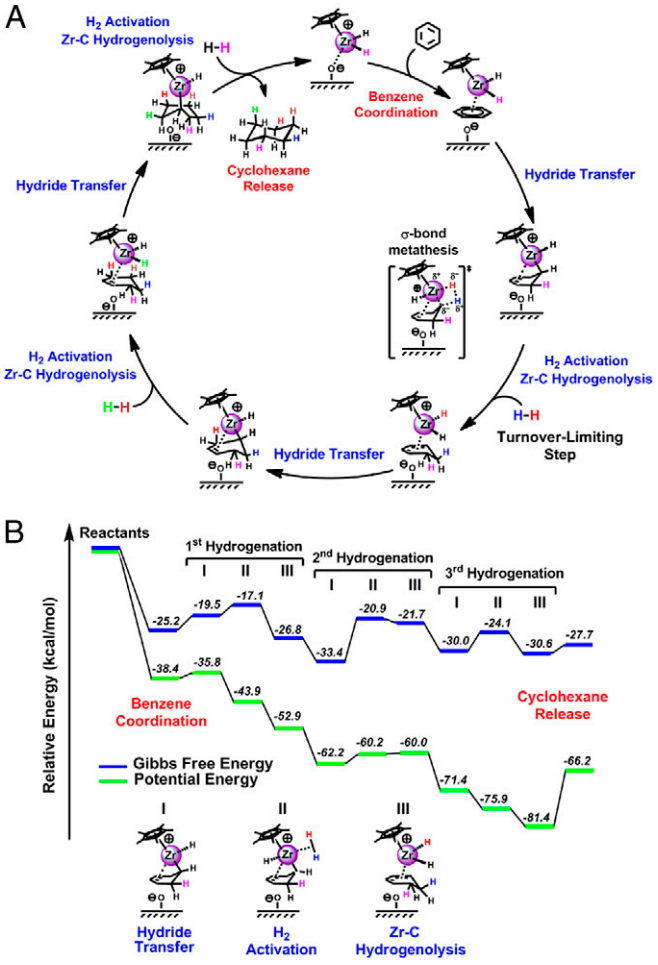

Fig. 6. Computed catalytic pathway for Cp*ZrH$_2^+$/AlS-mediated benzene hydrogenation. (*A*) Catalytic cycle. (*B*) Corresponding energetic profile. Sequences of three steps are operative following **Cp*ZrH$_2^+$/AlS** + benzene capture: I, hydride addition; II, H$_2$ activation; and III, Zr–C hydrogenolysis.

Materials and Methods

The procedure for the chemisorption of the organometallic complex Cp*ZrMe$_3$ on sulfated alumina was previously reported (18). For the synthesis and characterizations of the hydrogenolysis of Cp*Zr^{13}Me$_3$/AlS, dosing of Cp*ZrMe$_3$/AlS with benzene, benzene hydrogenation experiments with Cp*ZrMe$_3$/AlS, benzene hydrogenation experiment with Cp*ZrMe$_3$ + B(C$_6$F$_5$)$_3$, benzene hydrogenation experiment with Cp*ZrMe$_3$ + [Ph$_3$C][B(C$_6$F$_5$)$_4$], see *SI Materials and Methods*. For DFT calculations detaills, as well as EXAFS measurements and data analysis, also see *SI Materials and Methods*.

ACKNOWLEDGMENTS. We thank Dr. Jeremy Kropf for assistance with the EXAFS measurements and Dr. Weixing Gu for the homogeneous hydrogenation experiments. Research at Northwestern University was supported by the US Department of Energy Office of Science, Office of Basic Energy Sciences, under Grant DE-FG02-86ER13511 (L.A.W., M.D., and T.J.M.; catalyst synthesis, reactivity, and NMR spectroscopy). Use of NMR and GC-TOF at the IMSERC facility of Northwestern University was supported by NSF Grants CHE-1048773 and CHE-0923236. Use of the Advanced Photon Source was supported by the US Department of Energy, Office of Basic Energy Sciences, under Contract DE-AC02-06CH11357. MRCAT operations are supported by the Department of Energy and the MRCAT member institutions. J.T.M. and N.G.'s funding was provided by Chemical Sciences, Geosciences and Biosciences Division, US Department of Energy, under contract DE-AC0-06CH11357. DFT calculations were supported by the Ministero dell'Istruzione, dell'Università e della Ricerca (MIUR Rome). We acknowledge CINECA Award N. HP10BD82EA 2011 for providing computing resources and support.

1. Dal Santo V, Liguori F, Pirovano C, Guidotti M (2010) Design and use of nanostructured single-site heterogeneous catalysts for the selective transformation of fine chemicals. *Molecules* 15(6):3829–3856.
2. Thomas J-M, Raja R (2006) The advantages and future potential of single-site heterogeneous catalysts. *Top Catal* 40:3–17.
3. Williams L-A, Marks T-J (2011) Synthesis, characterization, and heterogeneous catalytic implementation of sulfated alumina nanoparticles. Arene hydrogenation and olefin polymerization properties of supported organozirconium complexes. *ACS Catal* 1:238–245.
4. Williams L-A, Marks T-J (2009) Chemisorption pathways and catalytic olefin polymerization properties of group 4 mono- and binuclear constrained geometry complexes on highly acidic sulfated alumina. *Organometallics* 28(1):2053–2061.
5. Eisen M-S, Marks T-J (1994) Recent developments in the surface and catalytic chemistry of supported organoactinides. *J Mol Catal* 86:23–50.
6. Wegener S-L, Marks T-J, Stair P-C (2012) Design strategies for the molecular level synthesis of supported catalysts. *Acc Chem Res* 45(2):206–214.
7. Hustad P-D (2009) Frontiers in olefin polymerization: Reinventing the world's most common synthetic polymers. *Science* 325(5941):704–707.
8. Makio H, Fujita T (2009) Development and application of FI catalysts for olefin polymerization: Unique catalysis and distinctive polymer formation. *Acc Chem Res* 42 (10):1532–1544.
9. Motta A, Fragaà IL, Marks T-J (2008) Links between single-site heterogeneous and homogeneous catalysis. DFT analysis of pathways for organozirconium catalyst chemisorptive activation and olefin polymerization on γ-alumina. *J Am Chem Soc* 130 (49):16533–16546.
10. Jezequel M, et al. (2001) Supported metallocene catalysts by surface organometallic chemistry. Synthesis, characterization, and reactivity in ethylene polymerization of oxide-supported mono- and biscyclopentadienyl zirconium alkyl complexes: Establishment of structure/reactivity relationships. *J Am Chem Soc* 123(15):3520–3540.
11. Joubert J, Delbecq F, Coperet C, Basset J-M, Sautet P (2008) Gamma-alumina: An active support to obtain immobilized electron poor Zr complexes. *Topics Catal* 48(1-4): 114–119.
12. Millot N, Soignier S, Santini C-C, Baudouin A, Basset J-M (2006) Synthesis, characterization, and activity in ethylene polymerization of silica supported cationic cyclopentadienyl zirconium complexes. *J Am Chem Soc* 128(29):9361–9370.
13. Popoff N, Gauvin R-M, De Mallmann A, Taoufik M (2012) On the fate of silica-supported half-metallocene cations: Elucidating a catalyst's deactivation pathways. *Organometallics* 31(13):4763–4768.
14. Fraenkel D, Jentzsch N-R, Starr C-A, Nikrad P-V (2010) Acid strength of solids probed by catalytic isobutane conversion. *J Catal* 274:29–51.
15. Arata K (2009) Organic syntheses catalyzed by superacidic metal oxides: Sulfated zirconia and related compounds. *Green Chem* 11:1719–1728.
16. Corma A (1995) Inorganic solid acids and their use in acid-catalyzed hydrocarbon reactions. *Chem Rev* 95(3):559–614.
17. Nicholas C-P, Marks T-J (2004) Zirconium hydrocarbyl chemisorption on sulfated metal oxides: New supports, chemisorption pathways, and implications for catalysis. *Langmuir* 20(22):9456–9462.
18. Nicholas C-P, Ahn H-S, Marks T-J (2003) Synthesis, spectroscopy, and catalytic properties of cationic organozirconium adsorbates on "super acidic" sulfated alumina. "Single-site" heterogeneous catalysts with virtually 100 active sites. *J Am Chem Soc* 125(14):4325–4331.
19. Profilet R-D, Rothwell A-P, Rothwell I-P (1993) Surface-supported group 5 metal organometallic compounds for catalytic arene hydrogenation. *J Chem Soc Chem Comm* 1:42–44.
20. Yang X, Stern C-L, Marks T-J (1994) Cationic zirconocene olefin polymerization catalysts based on the organo-lewis acid tris(pentafluorophenyl)borane. A synthetic, structural, solution dynamic, and polymerization catalytic study. *J Am Chem Soc* 116(22):10015–10031.
21. Ahn H, Nicholas C-P, Marks T-J (2002) Surface organozirconium electrophiles activated by chemisorption on "super acidic" sulfated zirconia as hydrogenation and polymerization catalysts. A synthetic, structural, and mechanistic catalytic study. *Organometallics* 21(9):1788–1806.
22. Wolczanski P-T, Bercaw J-E (1982) Alkyl and hydride derivatives of (pentamethylcyclopentadienyl)zirconium(IV). *Organometallics* 1(6):793–799.
23. Joubert J, et al. (2007) Synthesis, characterization, and catalytic properties of γ-Al_2O_3-supported zirconium hydrides through a combined use of surface organometallic chemistry and periodic calculations. *Organometallics* 26(14):3329–3335.
24. Yuzawa H, Aoki M, Itoh H, Yoshida H (2011) Adsorption and photoadsorption states of benzene derivatives on titanium oxide studied by NMR. *J Phys Chem Lett* 2(15): 1868–1873.
25. Noor A, Kretschmer W-P, Glatz G, Meetsma A, Kempe R (2008) Synthesis and structure of zirconium and hafnium polymerisation catalysts stabilised by very bulky aminopyridinato ligands. *Eur J Inorg Chem* 32:5088–5098.
26. Zuccaccia C, et al. (2004) NOE and PGSE NMR spectroscopic studies of solution structure and aggregation in metallocenium ion-pairs. *J Am Chem Soc* 126(5): 1448–1464.
27. Pellecchia C, Grassi A, Immirzi A (1993) Synthesis, crystal structure, and olefin polymerization activity of a zwitterionic h^6-arene zirconium tris(hydrocarbyl). *J Am Chem Soc* 115(3):1160–1162.
28. VandeVondele J, et al. (2005) QUICKSTEP: Fast and accurate density functional calculations using a mixed Gaussian and plane waves approach. *Comput Phys Commun* 167(2):103–128.
29. Liu Z-X, Somsook E, Landis C-R (2001) A (2)H-labeling scheme for active-site counts in metallocene-catalyzed alkene polymerization. *J Am Chem Soc* 123(12):2915–2916.
30. Guzei I-A, Stockland R-A, Jr., Jordan R-F (2000) The bis(η^5-cyclopentadienyl)methylzirconium(IV) methyltris(pentafluorophenyl)borate ion pair. *Acta Crystallogr C* 56(Pt 6):635–636.
31. Castagnola N-B, Kropf A-J, Marshall C-L (2005) Studies of Cu-ZSM-5 by X-ray absorption spectroscopy and its application for the oxidation of benzene to phenol by air. *Appl Catal A* 290(1–2):110–122.
32. Miller J-T, et al. (2006) The effect of gold particle size on Au-Au bond length and reactivity toward oxygen in supported catalysts. *J Catal* 240(2):222–234.
33. Chantler C-T (2004) Scattering factor calculations and dispersion corrections for heavy atoms. *J Phys Chem Solids* 65(12):1935–1941.
34. Allen F-H, Taylor R (2004) Research applications of the Cambridge Structural Database (CSD). *Chem Soc Rev* 33(8):463–475.
35. Hunter W-E, Hrncir D-C, Bynum R-V, Penttila R-A, Atwood J-L (1983) The search for dimethylzirconocene. Crystal structures of dimethylzirconocene, dimethylhafnocene, chloromethylzirconocene, and (μ-oxo)bis(methylzirconocene). *Organometallics* 2(6): 750–755.
36. DeBeer George S, Brant P, Solomon E-I (2004) Metal and ligand K-Edge XAS of organotitanium complexes: Metal 4p and 3d contributions to pre-edge intensity and their contributions to bonding. *J Am Chem Soc* 127(2):667–674.
37. Lyon JT, Andrews L (2006) Group 4 transition metal-benzene adducts: Carbon ring deformation upon complexation. *J Phys Chem A* 110(25):7806–7815.
38. Gillis D-J, Tudoret M-J, Baird M-C (1993) Novel arene complexes of titanium(IV), zirconium(IV), and hafnium(IV). *J Am Chem Soc* 115(6):2543–2545.
39. Ding F, Harman W-D (2004) Stereoselective tandem 1,4-addition reactions for benzenes: A comparison of Os(II), Re(I), and W(0) systems. *J Am Chem Soc* 126(42): 13752–13756.
40. Vedernikov A-N, Caulton K-G (2003) N-Pt^{IV}-H/N-H...Pt^{II} intramolecular redox equilibrium in a product of H-C(sp^2) cleavage and unusual alkane/arene C-H bond selectivity of ([2.1.1]pyridinophane)$Pt^{II}(CH_3)^+$. *Chem Commun* (3):358–359.
41. Schoenfeldt N-J, Ni Z, Korinda A-W, Meyer R-J, Notestein J-M (2011) Manganese triazacyclononane oxidation catalysts grafted under reaction conditions on solid cocatalytic supports. *J Am Chem Soc* 133(46):18684–18695.
42. Delgado M, et al. (2011) Characterization of surface hydride hafnium complexes on alumina by a combination of experiments and DFT calculations. *J Phys Chem C* 115(14):6757–6763.
43. Tada M, Muratsugu S, Kinoshita M, Sasaki T, Iwasawa Y (2010) Alternative selective oxidation pathways for aldehyde oxidation and alkene epoxidation on a SiO_2-supported Ru-monomer complex catalyst. *J Am Chem Soc* 132(2):713–724.
44. Bochmann M (2010) The chemistry of catalyst activation: The case of group 4 polymerization catalysts. *Organometallics* 29(21):4711–4740.
45. Chen E-Y-X, Marks T-J (2000) Cocatalysts for metal-catalyzed olefin polymerization: Activators, activation processes, and structure-activity relationships. *Chem Rev* 100(4):1391–1434.
46. Delferro M, Marks T-J (2011) Multinuclear olefin polymerization catalysts. *Chem Rev* 111(3):2450–2485.
47. Roberts J-A-S, et al. (2007) Diverse stereocontrol effects induced by weakly coordinating anions. Stereospecific olefin polymerization pathways at archetypal C_s)- and C_1)-symmetric metallocenium catalysts using mono- and polynuclear halo-perfluoroarylmetalates as cocatalysts. *J Am Chem Soc* 129(42):12713–12733.
48. Lanza G, Fragala I-L, Marks T-J (2002) Energetic, structural, and dynamic aspects of ethylene polymerization mediated by homogeneous single-site "constrained geometry catalysts" in the presence of cocatalyst and solvation: An investigation at the ab initio quantum chemical level. *Organometallics* 21(25):5594–5612.